ORGANOMETALLICS

Article pubs.acs.org/Organometallics

Ferrocene Adsorbed on Silica and Activated Carbon Surfaces: A Solid-State NMR Study of Molecular Dynamics and Surface Interactions

Patrick J. Hubbard, Jordon W. Benzie, Vladimir I. Bakhmutov,* and Janet Blümel*



Cite This: Organometallics 2020, 39, 1080-1091



ACCESS

Metrics & More

Article Recommendations

ABSTRACT: Ferrocene has been adsorbed on the surface of silica and activated carbon within the pores by dry grinding in the absence of a solvent at room temperature. While the dry adsorption and translational mobility of ferrocene within the pores are already established on the centimeter scale, there is little systematic understanding of the surface site-to-site motions of the ferrocene molecules and their orientation with respect to the surface. In this paper, silica and activated carbon, both widely applied in academia and industry as adsorbents, are used as support materials. Using variable-temperature 13 C and 2 H solid-state NMR and T_1 relaxation time measurements, the dynamics of ferrocene on the surfaces of silica and activated carbon within the pores has been quantitatively characterized on the molecular scale. The obtained data indicate that



ferrocene molecules show a liquid-like behavior on the surface. Fast exchange between isotropically moving molecules and surfaceattached molecular states of ferrocene has been found in samples with submonolayer surface coverages. The surface-attached molecular states have been characterized by the free energies ΔG^{\dagger} of 6.1 kcal/mol for silica and ΔG^{\dagger} of 6.2 kcal/mol for activated carbon at 223 and 263 K, respectively. The horizontally oriented ferrocene molecules are the most thermodynamically stable states on the surfaces of both materials. These molecules exhibit fast C_5 rotation of the Cp rings, as established by low-temperature 13 C and 2 H NMR. The interactions of ferrocene with the pore surfaces have been characterized by adsorption enthalpies measured as -8.4 to -7.0 kcal/mol and -6.7 kcal/mol for activated carbon and silica, respectively. It has been suggested that the ferrocene-surface interactions for both support materials have a polar character.

■ INTRODUCTION

Carbon allotropes play an important role in modern and future advances in science and engineering, and their importance cannot be overestimated. New carbon allotropes are still detected, as the recently discovered molecular C₁₈ rings show. Common applications range from the popular carbonsupported palladium catalyst to nanometer-scale electronics of the future. Importantly from an environmental perspective, organic and inorganic pollutants can be very efficiently adsorbed onto the surface of activated carbon, graphene oxide, and carbon nanotubes (CNT) from aqueous solution and gas streams.^{3–10} Recently, volatile odorous compounds (VOC) have been efficiently trapped on modified activated carbon surfaces.1

Activated carbon represents the most important allotrope that is applied on a large scale. It constitutes an indispensable sorbent in medicine and for catalysis and purification procedures. 12 Because it is less expensive in comparison to other carbon allotropes, it is employed in many commercially available forms. 12 Activated carbon is also environmentally benign, as it can be derived from biomass. 13 Furthermore, special activated carbon materials show promise for removing CO₂ from gas streams¹⁴ and heavy metals such as Hg²⁺, Cr⁶⁺ and Cd²⁺ and toxic organic contaminants from wastewater.^{3,4}

In general, the adsorption of small molecules on surfaces is important for processes in industry and academia that involve separation sciences and catalysis. NMR spectroscopic adsorption studies with activated carbon or other supports have focused mainly on liquids such as water, alcohols, and benzene. 15-17 2H NMR has, for example, been used to study alcohols confined in activated carbon fibers at low temperatures.¹⁷ Spectroscopic studies on adsorbed solids are more scarce. One example would involve phenanthrene adsorbed on biochars. 18 Solid-state NMR spectroscopy 19,20 is a powerful tool to investigate surface species: for example, immobilized catalysts on support surfaces.²¹ Furthermore, polycyclic aromatic hydrocarbons (PAH) have been adsorbed on silica² and studied by 13C solid-state NMR.23

The two most important anisotropic interactions that occur in the solid state and are utilized in NMR are the chemical shift anisotropy (CSA)^{19,20} and quadrupolar interactions.¹⁹ The

Special Issue: Organometallic Chemistry at Various Length Scales

Received: November 25, 2019 Published: March 5, 2020





CSA reflects the unsymmetry of the electronic surroundings of a nucleus. The spherically rather symmetric phosphonium salts, for example, have a small ³¹P CSA in the solid state, ^{21f,g} while polycrystalline phosphine oxides display a large CSA. 24,25 The same accounts for phosphines versus their metal complexes.²¹ A large CSA manifests in solid-state NMR spectra in the form of multiple sets of rotational sidebands in addition to the isotropic line when samples are rotated. The CSA parameters can be derived by simulations from the spectra of rotated samples or by measuring wide-line spectra without spinning. 19-21 In a case where a quadrupolar nucleus with nuclear spin I = 1 such as ²H or ¹⁴N is measured in the solid state, the large quadrupolar interactions lead to a Pake pattern. 19 The distance between the center lines of this Pake pattern can be used to determine the characteristic quadrupolar coupling constant. 19 In solution, both anisotropic interactions are completely averaged out and only the isotropic lines are seen in the spectra. However, in cases where the mobility is limited and only partial averaging occurs, the residual CSA and diminished quadrupolar coupling constant can be used to determine different modes of mobility, as described for ferrocene in the Results and Discussion.

We reported recently that species such as phosphine oxides²⁶ can be adsorbed on diverse surfaces by dry grinding, and we could demonstrate that they are mobile on silica surfaces.^{24,25} Regarding the adsorption of phosphine oxides on silica, the interactions with the surface are rather well-defined. The oxygen of the P=O functionality forms hydrogen bondes with surface silanol groups.^{24–26} Molecular hydrogen-bonded adducts of P=O groups with silanols,^{24,27} phenols,^{27,28} chloroform,²⁷ hydrogen peroxide,²⁹ and di(hydroperoxy)-alkanes³⁰ have all been identified by single-crystal X-ray diffraction.

Recently, we discovered that metallocenes of the type Cp_2M ($Cp = cyclopentadienyl, C_5H_5$) can be adsorbed on silica by dry grinding of the components in the absence of solvents. ^{31–33} In contrast to the phosphine oxides, hydrogen bonding can be excluded for the interactions of these metallocenes with silica or activated carbon surfaces. The interactions with the surfaces must be of a van der Waals type nature, but the orientation of ferrocene with respect to the surface is not yet known.

Under an inert atmosphere ferrocene does not undergo chemical reactions even with supports such as silica or alumina, in contrast to other types of metallocenes. In contrast, the important polymerization catalysts of the type Cp₂MCl₂ react readily via the chloride ligands when they are supported on silica^{34,35} or incorporated into polymers³⁶ or sol-gel-type materials.³⁷ However, even in the absence of chloride ligands, some of the Cp2M metallocenes react quickly with oxide surfaces after the adsorption step. On a silica or alumina surface, chromocene forms the important heterogeneous Union Carbide catalyst that is used industrially for olefin polymerization under mild conditions in the absence of a cocatalyst. 38,39 Despite the importance of this catalyst, its structure remains largely unknown. The commonly accepted partial structure of the catalytically active surface species consists of a CpCr^{III} moiety that must be bound to a surface siloxide anion, as determined by solid-state NMR⁴⁰ and XPS and IR studies.38

In our quest to elucidate the adsorption and subsequent reaction of the surface-bound chromium species, chromocene has been dry-ground with silica in the absence of a solvent that could influence the outcome of the surface reaction. 40 However, even without solvent the reaction is too fast and does not allow for sufficient time to study the initial elementary steps by solid-state NMR or other methods. Therefore, in the present work, we turned to the less reactive ferrocene that persists under inert gas for months with the same structure as chromocene. By obtaining a deeper insight about the dynamic processes of the adsorption of ferrocene on different surfaces, conclusions about the structurally similar chromocene should be possible. Especially the orientation of the ferrocene toward the surface is of interest, since the reaction, for example, with surface silanol groups can only take place after contact with the metal center, but not through the Cp ring. Any, albeit temporary, sideways orientation of a metallocene should facilitate the interaction of the metal with the surface. Regarding activated carbon surfaces, while there is no chemical reaction taking place when ferrocene or chromocene is adsorbed, comparing data from different surfaces allows for a complete quantitative analysis of the adsorption process by solid-state NMR spectroscopy. 31,40 Another incentive to study the interactions of Cp₂M-type metallocenes adsorbed in monolayers with support surfaces is related to the potential creation of single-atom catalysts by reducing the metal center.33

Previously, we have explored the dry adsorption of ferrocene and other robust metallocenes on the surfaces of activated carbon and silica²² only from a phenomenological perspective. 31-33 Even in the absence of solvents the metallocenes that have been adsorbed by dry grinding display dynamic effects. Accordingly, it could be demonstrated qualitatively with multinuclear dia- and paramagnetic solid-state NMR that metallocenes are mobile on the surface within the pores of amorphous silica and activated carbon. 31–33,40 It has been visualized on a centimeter length scale that ferrocene is translationally mobile in large silica gel specimens.³³ Importantly with respect to a later application in single-atom catalysis, 33 when the adsorption is undertaken in the absence of a solvent, well-defined monolayers are formed.³³ No stacking of metallocenes in multiple layers on the surface occurs on any support. ^{31–33} In case an excess of metallocene is offered, it remains in its polycrystalline form and does not adsorb.

Ferrocene and its derivatives are classic organometallic compounds that play a crucial role in such important fields as catalysis, stereoselective synthesis, and chiral chromatography. 41 Therefore, it is surprising that the knowledge about the interactions with surfaces of supports such as silica or activated carbon is rather limited. In fact, up to now, there is little intrinsic understanding of the behavior of ferrocene on the surface within the pores of silica and other adsorbents. $^{31-33}$ On the other hand, the molecular dynamics of ferrocene as a guest molecule in inclusion compounds has been well studied by Mössbauer and NMR spectroscopy. 42,43 For example, according to the ¹H line shape analysis and ¹H spin-lattice relaxation time measurements, ferrocene molecules, included in the structure of β -cyclodextrin, experience fast C_5 rotations of the Cp rings at the very low activation energy of $E_a = 0.8 \text{ kcal/}$ mol. 43 However, the overall isotropic reorientation of the ferrocene requires a much higher activation energy ($E_a = 10.7$ kcal/mol). 43 In contrast to such inclusion compounds, no details about reorientations of surface-adsorbed ferrocene molecules are known yet. Only isotropic reorientation has been described qualitatively at room temperature for ferrocene

on silica^{31,33} and activated carbon.³² Therefore, in this contribution we study the interactions of ferrocene molecules with silica and activated carbon surfaces and their dynamic behavior quantitatively.

Specifically, we apply variable-temperature 13 C and 2 H solid-state NMR 19,32,33,44,45 and T_1 relaxation time measurements 19 to investigate the behavior of ferrocene (Cp₂Fe, (C₅H₅)₂Fe; 1) and its deuterated derivative, Cp₂Fe- d_2 ((C₅H₄D)₂Fe; 2), in pores of silica (SiO₂) and activated carbon (AC) on the molecular scale. Using different support materials provides a deeper insight into the adsorption process itself and the ensuing mobilities of the surface species. These quantitative studies are of fundamental interest and have wide-ranging potential in fields such as heterogeneous catalysis, electronic devices, and the separation sciences.

■ RESULTS AND DISCUSSION

In this contribution, we sought to investigate the interactions of ferrocene with different support surfaces and their molecular dynamics quantitatively by solid-state NMR spectroscopy. A densely packed monolayer corresponds to 100% surface coverage. The amounts of ferrocene necessary to achieve this coverage have been determined earlier for the silica³³ and carbon³² brands used here. In the following we report the quantitative study of a silica sample with a 75% submonolayer surface coverage with ferrocene (1-75%-SiO₂) and an activated carbon sample with a 75% surface coverage (1-75%-AC). Deuterium-labeled ferrocene 2 has been investigated in samples with a 50% and 130% surface coverage (2-50%-AC and 2-130%-AC).

Unfortunately, IR spectroscopy is not a viable method to study dynamic effects. ⁴⁶ Ferrocene also does not have strong and characteristic Raman or IR bands ^{47–49} that would lie outside of the region where intense and broad absorption bands of the support materials reside. ^{50,51} For example, the prominent ferrocene bands (811, 1002, 1108, 1411, 3085 cm⁻¹) ⁴⁸ overlap with the broad and intense bands of activated carbon (800–1450, 3000–3600 cm⁻¹). ^{50,51}

However, solid-state NMR^{19,20} can be successfully applied to quantitatively characterize various molecular motions, when the reorientations in the magnetic field occur on the T_2 and/or T_1 relaxation time scale. The first case is based on temperature-dependent signal line shapes of target nuclei. In the second case relaxation time measurements can be used because the molecular reorientations correspond to the Larmor frequencies of the nuclei.

Some 13 C T_1 spin-lattice relaxation time measurements, carried out for samples of solid ferrocene and also for materials containing intercalated ferrocene molecules, have been reported previously. 52-54 It has been well established that the $^{13}\mathrm{C}$ T_1 relaxation times of ferrocene molecules are controlled by very fast reorientations of the Cp rings, recognized as C₅ rotations with very low activation energy. Therefore, these internal rotations can only be quantitatively characterized on the ${}^{13}C$ T_1 NMR time scale at extremely low temperatures. In fact, solid ferrocene shows a 13 C T_1 time temperature dependence, where a 13 C $T_{1 \, \text{min}}$ time is observed at 110 K,52 corresponding to an activation energy between 1.8 and 2.3 kcal/mol. Since the carbon spin-lattice relaxation times in solid ferrocene at room temperature and also at moderate temperatures are very long, they require long measurement times. This is not feasible for the characterization of our dilute samples that contain ferrocene only in

submonolayer quantities. Furthermore, as mentioned above, the $^{13}\mathrm{C}$ relaxation mechanism and its characteristics are already known for ferrocene-containing materials. Therefore, in this contribution we focus on the variable-temperature $^{13}\mathrm{C}$ and $^{2}\mathrm{H}$ solid-state NMR spectra, while the T_1 time measurements have been used only as diagnostic tests.

Figure 1 shows the ¹³C{¹H} MAS and static NMR spectra of polycrystalline ferrocene (1), recorded for comparison with the

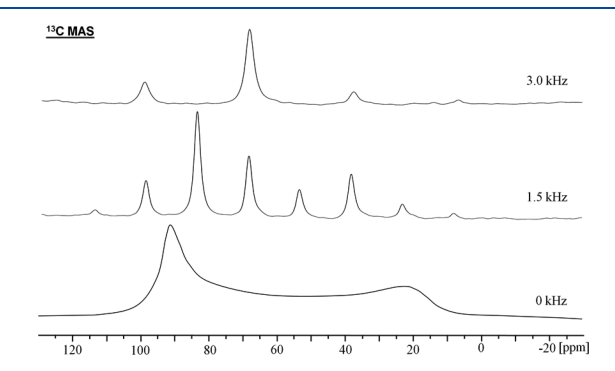


Figure 1. Room-temperature $^{13}C\{^1H\}$ NMR spectra of polycrystalline ferrocene (1) at the indicated MAS spinning speeds.

spectra of ferrocene molecules adsorbed on the surfaces in pores of the support materials. The static $^{13}C\{^1H\}$ NMR spectrum manifests a typical axially symmetric CSA (chemical shift anisotropy) pattern, 19,20 characterized by the parameters summarized in Table 1. Processing of the MAS NMR spectra

Table 1. 13 C Isotropic Chemical Shifts δ_{iso} and CSA parameters (CSA $\Delta\sigma$ and Asymmetry Parameter η) Derived from the 13 C 1 H 13 MAS and Static NMR Experiments Carried Out for 1, 1-75%-SiO $_{2}$, and 1-75%-AC

$\delta_{ m iso}$ (ppm)	$\Delta\sigma$ (ppm)	T (K)
68.6	$-54 \pm 2; \eta = 0$	298
69.9	0	298
68.4	$-52 \pm 2.0; \eta = 0.05$	180
68.1	0	298
68.5	\sim -55; $\eta = 0.2$	183
	68.6 69.9 68.4 68.1	68.6 -54 ± 2 ; $\eta = 0$ 69.9 0 68.4 -52 ± 2.0 ; $\eta = 0.05$ 68.1 0

led to parameters that are in excellent accordance with the theoretical and experimental studies of solid 1. On the basis of these studies, the static 13 C CSA pattern belongs to ferrocene molecules with the Cp rings rapidly rotating about their 5-fold symmetry axis. At this point it is important to emphasize that the Cp rings in solid 1 are magnetically equivalent.

Due to the fast Cp ring rotation, the 2 H NMR spectrum of static **2** shows the quadrupolar Pake pattern 19,32,26,44,45 with a quadrupolar splitting of 72 kHz (Figure 2). The fitting procedure (top spectrum in Figure 2) leads to the 2 H isotropic chemical shift $\delta_{\rm iso}$, which is set to 0 ppm, and a quadrupolar coupling constant $C_{\rm Q}$ of 98 \pm 2 kHz with an asymmetry parameter of $\eta=0.021$. These parameters agree well with those reported earlier. 32,56 As follows from the spectral data, the character of the dynamics of **2** does not change with temperature.

The material 1-75%-SiO₂ has been prepared by grinding the corresponding amount of 1 with silica (see the Experimental Section). This procedure could potentially change the structure of the host material. Therefore, ²⁹Si solid-state

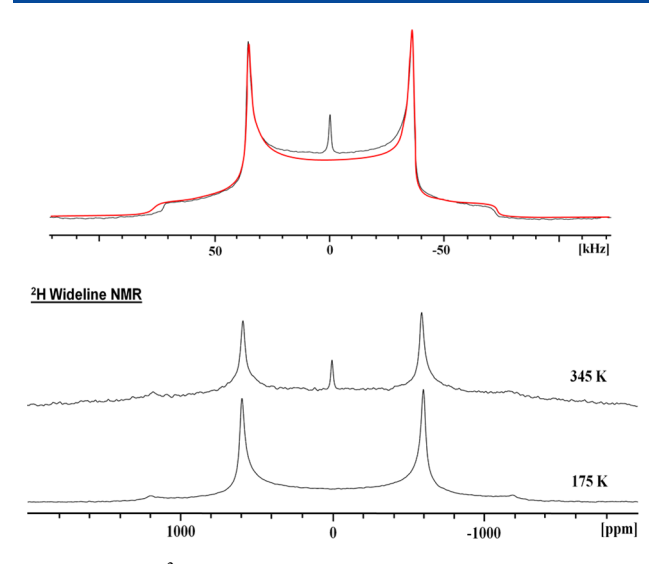


Figure 2. Static 2 H NMR of **2** at 345 and 175 K. The top spectrum shows the experimental and simulated static spectra at 295 K; the sharp signal in the center is an artifact appearing often in solid-echo experiments.

NMR spectra have been measured before and after grinding. Figure 3 shows the ²⁹Si{¹H} MAS NMR spectra recorded for

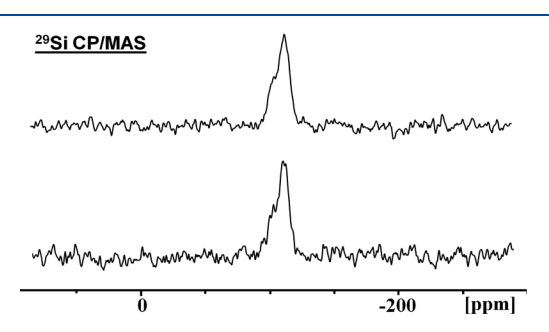


Figure 3. ²⁹Si{¹H} MAS NMR spectra of pristine dried silica (top) and 1-75%-SiO₂ (bottom), recorded at room temperature with a spinning rate of 3.1 kHz.

pristine silica and material 1-75%-SiO₂. Both spectra look practically identical and they exhibit two poorly resolved $^{29}\mathrm{Si}$ resonances at -103 and -112 ppm, representing $\mathrm{SiO_3}(\mathrm{OH})$ and $\mathrm{SiO_4}$ structural units 19,22c in about the same ratio. Therefore, a chemical reaction of 1 with the silica support, or a major structural change can be ruled out.

The static variable-temperature ¹³C{¹H} NMR spectra of the material **1-75%-SiO**₂, recorded at intervals of 10 K between 295 and 180 K, are presented in Figure 4. The evolution of the signal shapes with the temperature is fully reversible. In accordance with data reported earlier for ferrocene in silica³¹ and ferrocene inclusion compounds, ^{42,43} at ambient and moderately lower temperatures the spectrum manifests a sharp Lorentz-shaped resonance for the Cp rings at about 68 ppm. This feature demonstrates that an isotropic liquid-like reorientation of ferrocene in the pores of the material **1-75%-SiO**₂ takes place. The isotropic reorientation effectively averages out the CSA.

On the basis of this fact, and in contrast to inclusion compounds studied earlier, 6,43,53 which contain a single ferrocene molecule in the structural unit, two different motional modes can be suggested for interpreting the sharp carbon resonance in the $^{13}C\{^1H\}$ NMR spectra (Figure 4).

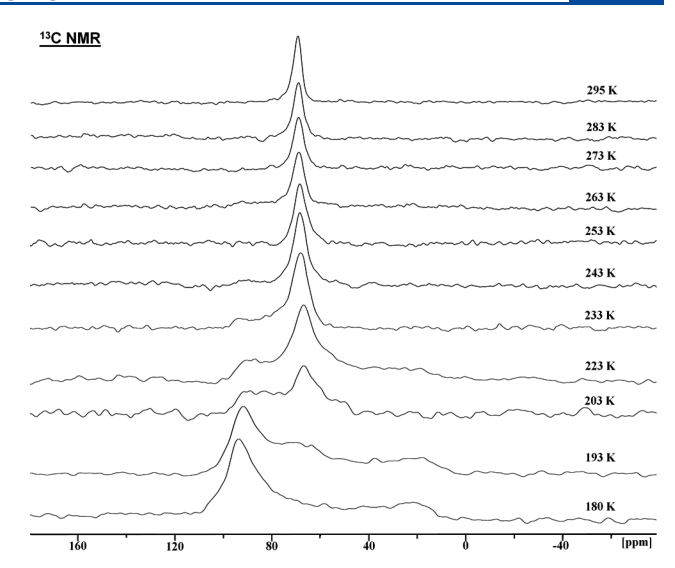
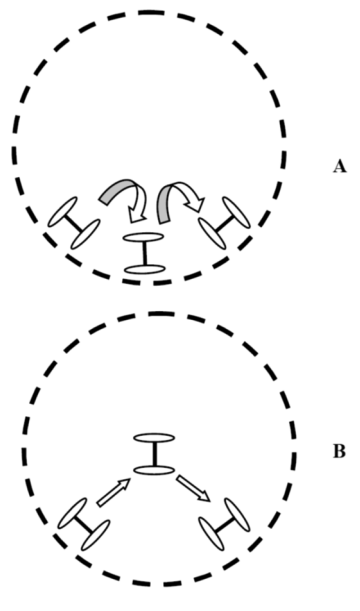


Figure 4. ¹³C{¹H} NMR spectra of the static sample 1-75%-SiO₂ recorded at the indicated temperatures.

The first model (Scheme 1A) corresponds to the ferrocene motions occurring along the pore surface and can be imagined

Scheme 1. Two Potential Motional Modes Leading to a Sharp Carbon Resonance of Ferrocene in 1-75%-SiO₂^a



^aThe broken line circles indicate the surfaces of idealized pores of the support.

as a "tumbleweed scenario". Here, the bound horizontal molecular state of the ferrocene transforms to the vertical state and back again to the horizontal state. In combination with the Cp rotations around the C_5 symmetry axis, these motions will imitate isotropic reorientations. It should be noted that recently both molecular orientations have been found for ferrocene, physically adsorbed on a metal surface, by low-temperature scanning tunneling microscopy and density functional theory calculations. The second model (Scheme 1B) corresponds to a chemical exchange between the bound horizontal state (see below) and truly isotropically moving ferrocene molecules.

The choice between the models A and B in Scheme 1 for the mobility of 1 on the surface can be made by considering the temperature-dependent $^{13}\text{C}\{^1\text{H}\}$ NMR spectra in Figure 4. Upon cooling, the sharp carbon resonance experiences an evolution to show the axially symmetric CSA pattern at 180 K, belonging to immobile ferrocene molecules. As follows from the data reported in Table 1, the CSA parameters of this pattern and 1 at 298 K (Figure 1) are practically identical. Thus, surface-bound ferrocene molecules also experience fast Cp rotations around the C_5 symmetry axis.

The following spectral features in Figure 4 are important in the context of the motional models described above (Scheme 1). (a) The CSA pattern and the isotropic line coexist at low temperatures. This is especially obvious in the spectra recorded at 223, 203, and 193 K. (b) The resonances show chemical exchange on the NMR time scale, as evidenced by the reversibility of the signal evolution. (c) The line width and shape of the narrow resonance do not change when the sample is cooled, while the CSA pattern of a distinct separate signal appears. This again speaks for a slow exchange between the isotropic and bound states that occurs on the NMR time scale and allows van't Hoff analyses (see below). This result is only compatible with model B (Scheme 1), as model A would lead to one averaged signal that broadens gradually upon cooling. The analogous interpretation accounts for the results of the variable-temperature ²H NMR spectra discussed below. (d) The relative populations of the resonances change with the temperature. In addition, a single ferrocene- d_5 molecule, included into a thiourea matrix, 42 does not show the temperature evolution of the ²H resonance between 221 and 172 K, corresponding to motions of the ferrocene molecule itself, on the NMR time scale. Thus, the experimental data only support the motional model B well (Scheme 1).

Several ¹³C{¹H} MAS NMR experiments were performed with different spinning speeds for 1-75%-SiO₂ at 180 K (Figure 5). As can be deduced from the MAS spectra, one single isotropic ¹³C resonance at 68 ppm is observed at 180 K, corresponding to both magnetically equivalent Cp rings. In accordance with this observation, the simulation of the CSA pattern in the top trace of Figure 5 can be reached only by assuming the presence of one single Cp resonance. Assuming a vertical orientation of the surface-attached ferrocene molecules, the π electrons of one of the Cp rings are supposed to interact with the surface of silica, leading to nonequivalency of the Cp rings in the ¹³C{¹H} MAS NMR spectra. Both Cp rings in vertical molecular states could in principle participate in this interaction if the pore sizes of the silica were only about 7-9 Å. This would be in the range of the height of ferrocene, which is 6.7 Å, when the van der Waals radii of the carbon atoms are included. However, the average pore diameter of the silica used is 40 Å. Therefore, due to the equivalency of the Cp rings in the ¹³C{¹H} NMR spectrum of 1-75%-SiO₂ at 180 K, the horizontally oriented molecular states are much more likely. Finally, since the isotropically moving component is completely absent in the ¹³C{¹H} NMR spectra at 180 K (Figure 4), these horizontally oriented state ferrocene molecules, interacting with the surface of silica within the pores, are the most thermodynamically stable.

As seen in Figure 4, the signal intensity of the isotropic component increases with the temperature. The experimental and simulated ¹³C{¹H} NMR spectra of 1-75%-SiO₂ at 233 K are shown in Figure 6. From these, the mole fractions of both components can be determined by deconvolution. Using this

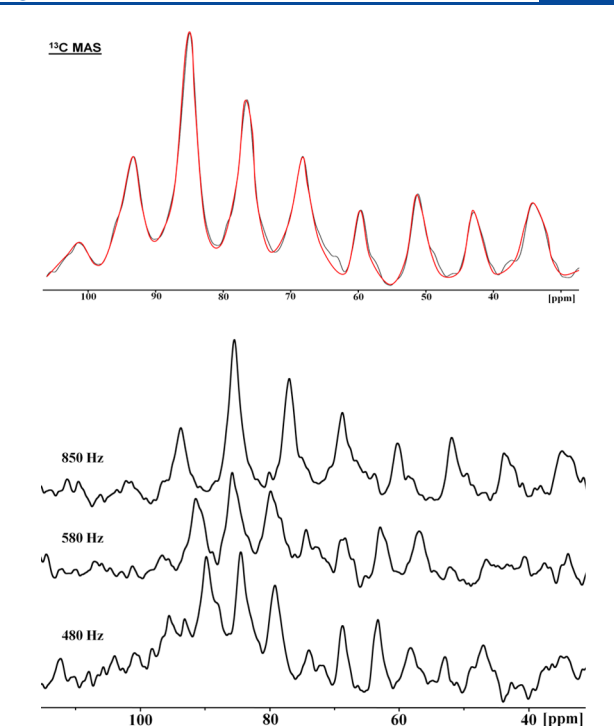


Figure 5. 13 C 14 H MAS NMR spectra of 1-75%-SiO $_{2}$ recorded at 180 K with the indicated spinning speeds. The top spectrum shows the simulation of the spectrum obtained at 850 Hz, corresponding to the CSA parameters given in Table 1.

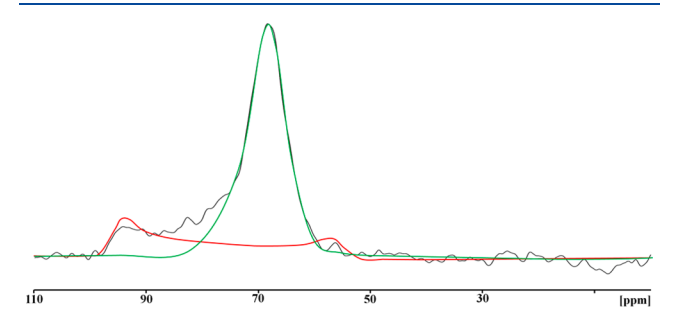


Figure 6. Simulation of the $^{13}C\{^{1}H\}$ NMR spectrum of 1-75%-SiO₂ at 233 K. The large isotropically moving component is represented by the green line, and the low-intensity CSA pattern of the surface-attached ferrocene molecules is drawn in red.

approach, the fractions of the surface-attached molecules $(P_{\rm bound})$ and the isotropically moving molecules $(P_{\rm iso})$, found between 193 and 233 K, lead to the calculated equilibrium constants $(K_{\rm eq}=P_{\rm iso}/P_{\rm bound})$. The latter, summarized in Table 2, describe the transformation of bound to isotropically moving molecules. Then, the slope of the dependence of ln $K_{\rm eq}$ versus 1/T (Figure 7) allows us to determine the enthalpy that

Table 2. Temperature Dependence of the Mole Fractions Found for Isotropically Moving Molecules of 1 ($P_{\rm iso}$) and Surface-Bound Molecules ($P_{\rm bound}$) in 1-75%-SiO₂ and the Corresponding Equilibrium Constants ($K_{\rm eg}$)

T (K)	$P_{\rm iso}$	$P_{ m bound}$	$K_{ m eq}$
193	0.0898	0.9102	0.0987
203	0.280	0.720	0.389
223	0.405	0.595	0.681
233	0.763	0.237	3.219

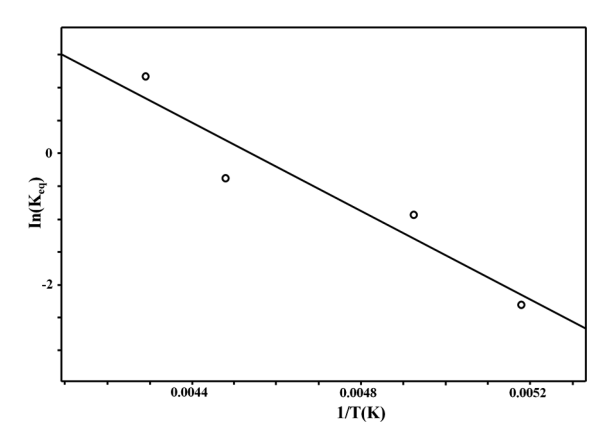


Figure 7. Temperature dependence of the equilibrium constant $(K_{\rm eq})$ depicted as $\ln K_{\rm eq}$ versus 1/T, obtained for the sample 1-75%-SiO₂.

characterizes the ferrocene/silica surface interactions via the adsorption enthalpy of 1, which can be calculated as $\Delta H^\circ = -6.7 \pm 0.5$ kcal/mol with a ΔS° value of +30 \pm 2 eu. It should be noted at this point that the positive entropy change corresponds well to the increased randomness of the isotropic state.

As outlined above, the static 13 C{ 1 H} NMR resonances in Figure 4 show chemical exchange between the surface-attached and isotropically moving molecules of **1** within the silica pores, taking place on the T_2 NMR time scale. A quantitative line shape analysis in these spectra is obviously difficult. However, the 13 C line shape observed at 223 K provides an estimate of the rate constant $k_{\rm exch}$ as $19 \times 10^3 \ {\rm s}^{-1}$ within the limits of a three-center exchange. This value then gives a $\Delta G(223 \ {\rm K})^{\ddagger}$ value of 6.1 kcal/mol for the exchange.

In principle, the ¹³C NMR signal obtained at 180 K (Figure 4) could also stem from recrystallized 1 instead of molecules attached to the silica surface. The values in Table 1 show that the ¹³C NMR parameters of polycrystalline 1 and surfaceattached ferrocene molecules in 1-75%-SiO2 are practically the same. Therefore, regarding only adsorption on one support material, there is no strong evidence that the immobile molecules are indeed located on the surface within the pores of silica, and not in crystallized 1. However, independent evidence and clarification regarding the different scenarios can be obtained by probing the material 1-75%-AC because activated carbon, being paramagnetic, is active in EPR spectroscopy. In accordance with the paramagnetic nature of this support, the 13 C T_1 times determined for the Cp rings in a static sample of 1-75%-AC are extremely short with 0.05 s (298 K), 0.06 s (283 K), and 0.06 s (273 K). In comparison, the 13 C T_1 relaxation times are longer than 18 s in polycrystalline 1. Therefore, it can be assumed that the Cp rings are in contact with the surface of the activated carbon support.

The temperature evolution of the ¹³C{¹H} NMR resonances in the spectra of static 1-75%-AC (Figure 8) is similar to that observed for 1-75%-SiO₂. At the static regime the ¹³C resonance of the activated carbon support is very broad and can be eliminated by a baseline correction. In analogy to the case of 1 on silica, the isotropic resonance of ferrocene in 1-75%-AC, observed at 298 K with the chemical shift reported in Table 1, transforms to the CSA pattern at 183 K. However, in contrast to 1-75%-SiO₂, the pattern is broadened significantly. In fact, the simulation of this CSA pattern (Figure 8, top) requires now a line width larger than 1.2 kHz with the

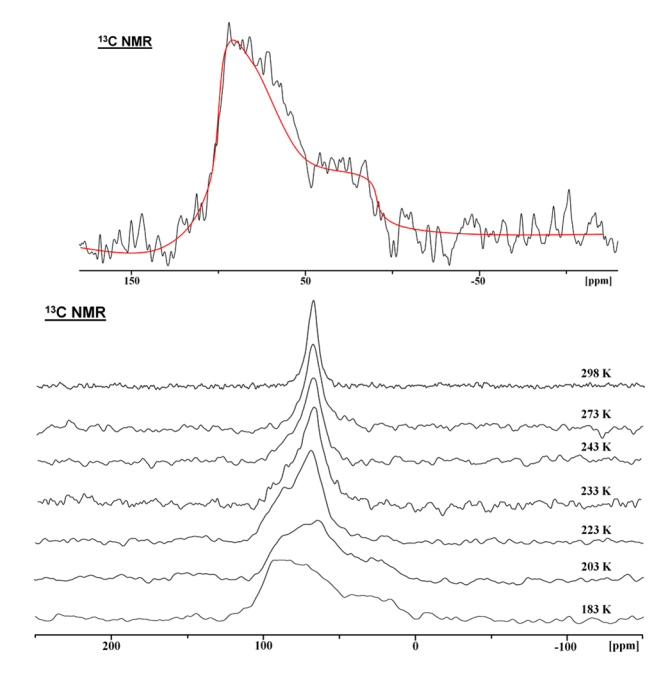


Figure 8. Variable-temperature $^{13}C\{^1H\}$ NMR spectra of a static sample of 1-75%-AC at the indicated temperatures. The top trace shows the CSA simulation of the signal at 183 K.

parameters summarized in Table 1. This broadening is obviously caused by strong dipolar electron—nucleus interactions between 1 and the paramagnetic surface of the activated carbon, preventing a quantitative analysis of the spectra. This problem can be avoided by studying the material 2-50%-AC, containing a deuterium label, which is less sensitive to paramagnetic effects. Figure 9 shows the variable-temperature ²H NMR spectra obtained from a static sample of 2-50%-AC.

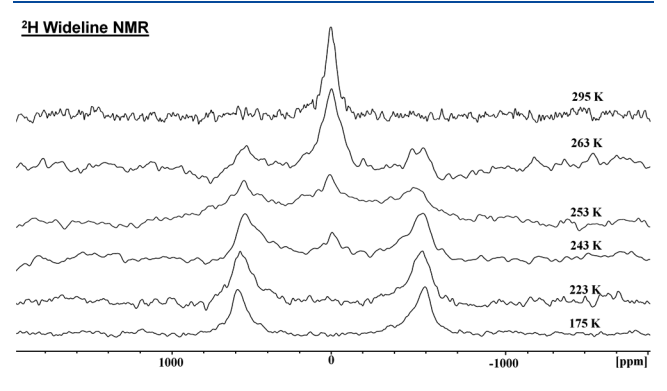


Figure 9. Variable-temperature ²H NMR spectra of a static sample of **2-50%-AC** recorded at the indicated temperatures.

In accordance with the ¹³C NMR data in Figure 8, the spectrum exhibits a single deuterium resonance at 295 K, belonging to isotropically moving ferrocene molecules. Upon cooling, this resonance turns into a quadrupolar pattern ¹⁹ similar to that of solid 2 in Figure 2, which can be simulated with the quadrupolar parameters $C_Q = 98 \pm 3$ kHz and $\eta = 0.08$. The same pattern, observed at low temperatures, has been reported for deuterated ferrocene $(C_5D_5)_2$ Fe placed into a thiourea matrix. ⁴² In analogy to the case of 2, the low-temperature quadrupolar pattern of 2-50%-AC does not show features that could be interpreted as nonequivalency of the Cp

rings. Thus, a vertical molecular stance of ferrocene on the activated carbon surface is not probable. The line broadening in the ²H low-temperature spectrum (Figure 9) is most likely due to interactions with electrons of the paramagnetic activated carbon support, as described above for the ¹³C nuclei.

The variable-temperature ²H NMR spectra of **2-50%-AC** in Figure 9 demonstrate the absence of the isotropic component at 175 K, which grows gradually, however, upon heating.

The ²H NMR spectrum, recorded at 263 K and simulated as a superposition of the quadrupolar pattern and the isotropic component, is illustrated in Figure 10. It should be noted that

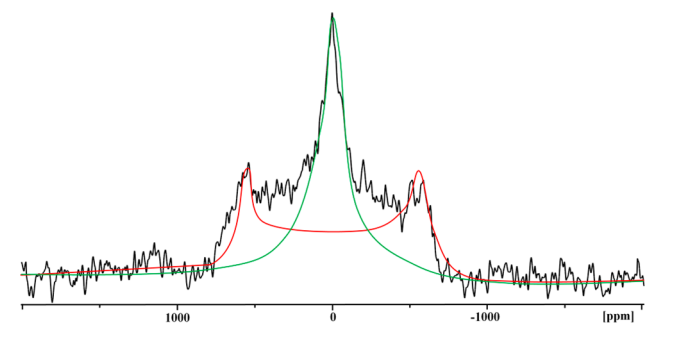


Figure 10. Static 2 H NMR spectrum of **2-50%-AC** at 263 K. The red line shows the simulation of the quadrupolar pattern with $C_{\rm Q}=97$ kHz and $\eta=0.08$, and the green line depicts the isotropic component.

this simulation requires the line width of both components to be 5.5 kHz versus 1 kHz used for the FID treatment. As in the case of the $^{13}\mathrm{C}\{^1\mathrm{H}\}$ NMR spectra of 1-75%-SiO₂, deconvolution leads to mole fractions of the isotropically moving ferrocene molecules (P_{iso}) and surface-attached molecules (P_{bound}). These give, in turn, the equilibrium constants $K_{\mathrm{eq}} = P_{\mathrm{iso}}/P_{\mathrm{bound}}$ summarized in Table 3. A

Table 3. Temperature-Dependent Mole Fractions of Isotropically Moving Ferrocene Molecules $(P_{\rm iso})$ and Surface-Attached Molecules $(P_{\rm bound})$ and the Corresponding Equilibrium Constants $(K_{\rm eq})$ Determined for 2-50%-AC

T (K)	$P_{ m iso}$	$P_{ m bound}$	$K_{ m eq}$
243	0.078	0.922	0.085
247	0.11	0.89	0.124
253	0.146	0.854	0.171
263	0.25	0.75	0.33

comparison of the values in Table 3 with those in Table 2 clearly indicates the difference between the silica versus the activated carbon support. For example, $K_{\rm eq} = P_{\rm iso}/P_{\rm bound}$ for ferrocene adsorbed on silica at 233 K equals 3.2 (Table 2), while it is 0.085 for activated carbon as the support at 243 K (Table 3). In spite of the small temperature difference, $K_{\rm eq}$ is orders of magnitude larger for silica than for the activated carbon sample.

The straight line in coordinates $\ln K_{\rm eq}$ versus 1/T in Figure 11 leads to the absorption enthalpy of ferrocene molecules in AC, an ΔH° value of -8.4 ± 1.0 kcal/mol, and a ΔS° value of 30 ± 3 eu. Finally, the additional line broadening, found at the simulation of the spectrum in Figure 10, is most likely caused by a chemical exchange between surface-attached and isotropically moving molecules in the material 2-50%-AC. This exchange, resulting in the single sharp resonance in the room-temperature 2 H NMR spectrum, could be characterized

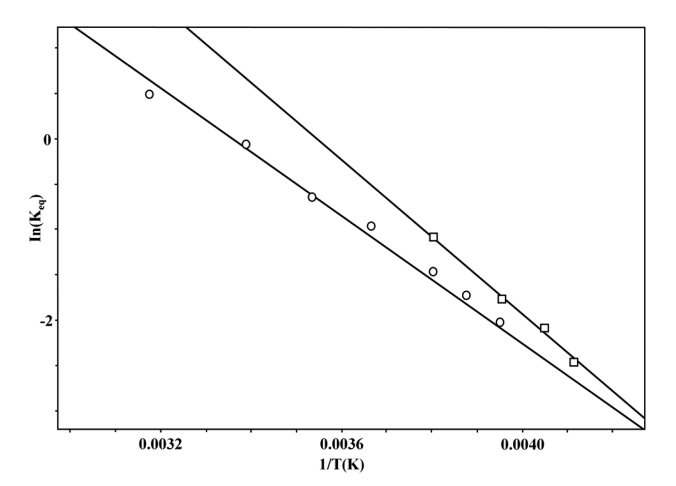


Figure 11. Temperature dependence of the equilibrium constant $K_{\rm eq}$ depicted as $\ln K_{\rm eq}$ versus 1/T, obtained from the samples 2-50%-AC (\Box) and 2-130%-AC (\bigcirc).

by the rate constant $k_{\rm exch}$ of $145 \times 10^3 \, {\rm s}^{-1}$ at 263 K within the limits of a three-center exchange, giving $\Delta G(263 \, {\rm K})^{\ddagger} = 6.2 \, {\rm kcal/mol}$. This value is close to the 6.1 kcal/mol obtained for the material 1-75%-SiO₂.

In the context of the present study, the material 2-130%-AC, prepared with a 130% coverage of the surface, was of great interest. Figure 12 shows the room-temperature ¹³C{¹H} MAS

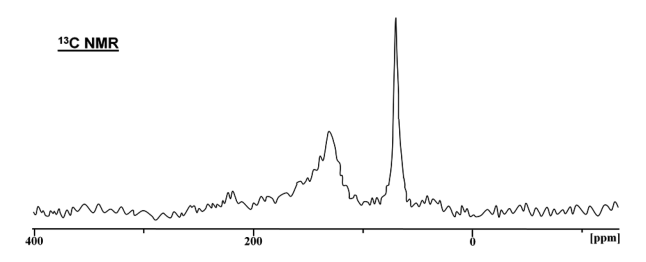


Figure 12. $^{13}C\{^{1}H\}$ MAS NMR spectrum of 2-130%-AC at a spinning speed of 9 kHz.

NMR spectrum of this material, recorded with a spinning speed of 9 kHz. The broad resonance at 129 ppm can be attributed to carbon nuclei of the activated carbon support, while the relatively sharp line belongs to the Cp rings of 2. As in the case of 1-75%-AC, the 13 C $T_{\rm 1}$ time of the Cp ring carbon nuclei is only 0.056 s, which is close to the value of 0.08 s measured for the carbons of activated carbon. The extremely fast relaxation of the Cp rings in 2-130%-AC supports again the assumption that ferrocene molecules are actually located in the pores of this paramagnetic material in spite of being present in excess of a monolayer in the sample. The variable-temperature 2 H NMR spectra of the static sample 2-130%-AC (Figure 13) overall resemble those displayed in Figure 9. Nevertheless, the following features deserve additional attention.

First, even at 315 K, the ²H NMR spectrum exhibits a low-intensity pattern with a quadrupolar splitting, corresponding to surface-attached ferrocene molecules or polycrystalline 2 (see Figure 2), located within the pores of the support. Note that this quadrupolar pattern is especially visible in the form of sidebands in the ²H MAS spectrum of 2-130%-AC (Figure 13, top). Second, in contrast to the ferrocene in the material 2-50%-AC with a submonolayer of 2, the chemical exchange

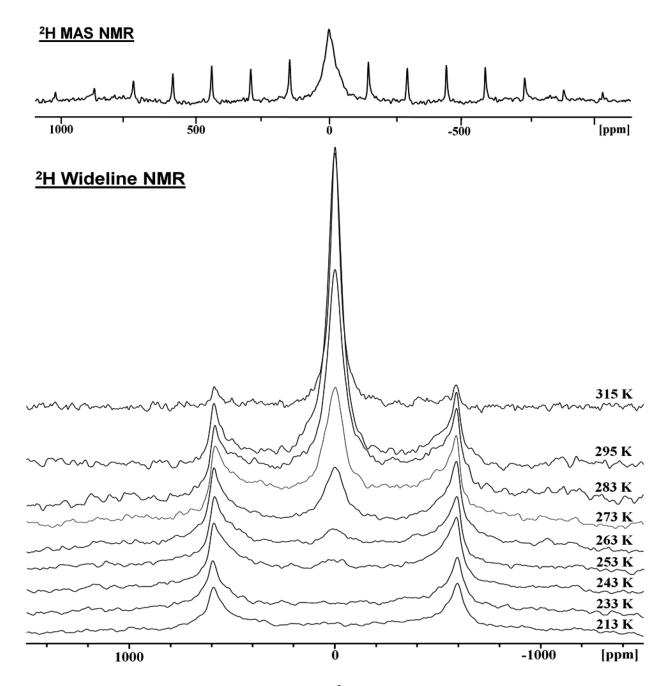


Figure 13. Variable-temperature ²H NMR spectra collected for a static sample of **2-130%-AC** at the indicated temperatures (bottom). The top spectrum is the room-temperature ²H MAS NMR of **2-130%-AC**, spinning at a rate of 9 kHz.

between liquid-like molecules and surface-bound molecules is slow on the NMR time scale. In the context of this exchange, this result is quite reasonable because decreasing the free space on the activated carbon pore surface by increasing the total amount of 2 will impede the exchange. Third, in spite of 2 being present in excess of a monolayer, the ²H NMR spectra of 2-130%-AC recorded at the lowest temperatures do not manifest the isotropic resonance. This effect can be attributed to the formation of a second layer of the ferrocene on the pore surface.

To determine the mole fractions of the isotropically moving ferrocene molecules $(P_{\rm iso})$ and surface-attached molecules $(P_{\rm bound})$ in **2-130%-AC**, we have used the approach described above for **2-50%-AC**. The fractions and equilibrium constants, defined again as $K_{\rm eq} = P_{\rm iso}/P_{\rm bound}$, are summarized in Table 4. Figure 11 displays the corresponding correlation yielding the thermodynamic parameters ΔH° (-7.03 ± 0.6 kcal/mol) and ΔS° (36 ± 3 eu). The somewhat reduced adsorption enthalpy ΔH° on going from **2-50%-AC** to **2-130%-AC** can be explained by the formation of a second layer of **2** on the

Table 4. Temperature-Dependent Mole Fractions of Isotropically Moving Ferrocene Molecules $(P_{\rm iso})$ and Surface-Attached Molecules $(P_{\rm bound})$ and the Corresponding Equilibrium Constants $(K_{\rm ed})$ Determined for 2-130%-AC

T (K)	$P_{ m iso}$	$P_{ m bound}$	$K_{ m eq}$
243	0.050	0.95	0.053
253	0.117	0.883	0.133
258	0.151	0.849	0.178
263	0.187	0.813	0.230
273	0.276	0.724	0.381
283	0.342	0.658	0.519
295	0.484	0.516	0.938
315	0.620	0.38	1.632

surface. One might speculate that two layers of ferrocene are, in a solid-state NMR sense, equivalent to polycrystalline 2 within the pores.

Since the quadrupolar patterns of the individual deuterated ferrocene molecules in polycrystalline 2 and surface-attached molecules in 2-50%-AC and 2-130%-AC at low temperatures are practically identical, it was important to determine the difference between them by measuring the ${}^{2}H$ T_{1} times in static samples of 2 and 2-130%-AC. The 2H NMR T_1 relaxation data obtained for 2 at different temperatures are 1.10 s (295 K), 0.70 s (263 K), 0.67 s (258 K), 0.39 s (213 K), and 0.15 s (185 K). To show that these values are correct, they have been presented as a correlation of $\ln T_1$ versus $1/T_2$, giving a straight line which corresponds to an activation energy of 1.9 kcal/mol for the relaxation process. Therewith, the activation energy lies in the region of 1.8-2.3 kcal/mol, reported for the fast C_5 rotation of the Cp rings. ^{43,52} For a static sample of 2-130%-AC, the ${}^{2}H$ T_{1} measurements were reliable at low temperatures, when only the quadrupolar signal was observed, resulting in the values 0.09 s (213 K) and 0.04 s (185 K). The T_1 measurement at 295 K was successful for a spinning sample of 2-130%-AC by using the sideband pattern (Figure 13, top) to result in a 2 H T_{1} time of 0.35 s. Obviously, on going from 2 to 2-130%-AC, the ${}^{2}H$ T_{1} time shortens significantly. This illustrates that dipolar electron-nucleus interactions between the ferrocene molecules and the paramagnetic surface of the activated carbon occur. We consider this effect as an additional proof that the ferrocene molecules reside on the surface within the pores of the activated carbon support.

Finally, a fourth feature in the ²H NMR spectra of 2-130%-AC in Figure 13 deserves a more detailed discussion. The line width of the central, isotropic component of the spectrum is large, growing from 3.3 kHz at 315 K to 8.2 kHz at 273 K, while the quadrupolar pattern practically does not change. This "selective" broadening is visible best in the MAS NMR spectrum (Figure 13, top), where the broadened isotropic line is observed in combination with the sideband pattern containing sharp lines. This feature has been noticed earlier³² and attributed to the higher translational mobility of the adsorbed molecules of 2 upon heating the samples. However, the same spectroscopic effect can appear when the isotropically moving molecules experience a very fast chemical exchange with additional molecular states, acting as intermediates in the slower exchange with the horizontally bound molecules. We suggest that the vertically oriented (semibound) molecules represent such intermediates. This explanation can be supported by the following observations. First, the broadening of the isotropic resonance does not show quadrupolar features, which would appear in the case of slowing down translational motions at low temperatures. Second, the ${}^{2}H$ T_{1} time of 0.021 s measured for the central component in the MAS spectrum (Figure 13) at 295 K cannot provide the experimentally observed line width of 4.3 kHz.

In summary, liquid-like behavior has been found for ferrocene molecules residing on silica and activated carbon surfaces within the pores. In both materials, the surface-attached adsorbed ferrocene molecules have been recognized as horizontally oriented thermodynamically stable states, experiencing fast rotations around the C_5 symmetry axis of the equivalent Cp rings, while the vertically oriented states can play a role as intermediates in the exchange between surface-attached and detached ferrocene molecules.

The horizontally oriented molecular states obviously do not promote the possible formation of hydrogen bonds of the type Si-O-H··· π -electrons on the silica surface as well as $\pi-p$ interactions of ferrocene with hexagonal and pentagonal rings of the activated carbon. Since the iron atoms in ferrocene molecules have a partial positive charge, their interactions with the surfaces of both silica and activated carbon are of a polar nature.

Adsorption enthalpies and energies of surface-adsorbate interactions depend significantly on the host structures and pore sizes. 63-66 Therefore, it is difficult to compare the thermodynamic parameters obtained for the adsorption of ferrocene on silica and activated carbon surfaces. The same accounts for other adsorbates in the pores of different support materials. However, it is interesting that, in contrast to the $K_{\rm eq}$ values for silica and activated carbon, the enthalpies characterizing the ferrocene-surface interactions are similar for silica (-6.7 kcal/mol) and for activated carbon (-8.4 to -7.0 kcal/mol)mol). In fact, the value obtained for silica is very close to the heat of adsorption of benzene in microporous SiO_2 (-6.7 kcal/ mol).⁶⁴ At the same time, the interactions between ferrocene and activated carbon strongly exceed π -p interactions of benzene molecules in the pores of activated carbon (-4.2 kcal/ mol).11

CONCLUSION

In this contribution variable-temperature ¹³C and ²H solidstate NMR experiments have been performed to characterize the dynamics of ferrocene molecules adsorbed on the surface within the pores of silica and activated carbon. Ferrocene shows a liquid-like behavior in the pores of both supports. It has been demonstrated that isotropically moving molecules and surface-attached molecular states of the ferrocene experience chemical exchange. The exchange is fast on the NMR time scale in the samples 1-75%-SiO₂ and 1-75%-AC and also in 2-50%-AC with submonolayer surface coverages. This exchange has been characterized by the free energy values of $\Delta G^{\ddagger} = 6.1$ kcal/mol for silica and $\Delta G^{\ddagger} = 6.2$ kcal/mol for activated carbon at 223 and 263 K, respectively. In contrast to the submonolayer coverages, the material 2-130%-AC, containing an excess of the ferrocene, shows a slow exchange. This indicates that vacant surface sites are indispensable for this exchange to take place.

The thermodynamically most stable state of ferrocene and ferrocene- d_2 on the surface within the pores of both materials is the horizontally oriented state. This state is directly observed at low temperatures, while fast rotation of Cp rings around their C_5 symmetry axis takes place. The adsorption enthalpies of ferrocene in the pores of activated carbon and silica have been determined as -8.4 to -7.0 kcal/mol and -6.7 kcal/mol, respectively. It has been suggested that interactions of the adsorbed ferrocene with the surface are of a polar nature in both materials. The new insights gained on this research topic should have major implications for catalysis, as adsorption is the first step in generating many heterogeneous metallocene-based catalysts on supports: for example, the Union Carbide catalyst.

EXPERIMENTAL SECTION

Materials. The silica (Merck, 40 Å average pore diameter, 0.063–0.2 mm average particle size, specific surface area 750 m²/g) was dried in vacuo at 200 °C for 2 days to remove adsorbed water and condense surface silanol groups. 22

The activated carbon DARCO KB-G was obtained from Sigma-Aldrich, and it has a specific surface area of $1700 \text{ m}^2/\text{g}$ and pore volumes for micro-, meso-, and macropores of 0.36, 0.95, and 0.45 mL/g, respectively. Batches were predried and degassed for 3 h at 200 °C *in vacuo* (0.035 mmHg) prior to being weighed in and used for adsorbing ferrocene.

Sample Preparation. The maximum surface coverage of the silica with 1 has been determined earlier. The sample 1-75%-SiO₂ was prepared by dry grinding of 355.0 mg (1.908 mmol) of Cp₂Fe (1) with 1 g of silica for 5 min using a pestle and mortar. The deuterated ferrocene Cp₂Fe-d₂ (2) was synthesized by double lithiation and subsequent quenching with D₂O according to a literature method. The sample 2-75%-SiO₂ was created by dry grinding of 2 (355.0 mg, 1.887 mmol) with 1 g of silica. The maximum monolayer surface coverage of the activated carbon brand DARCO KB-G has been determined previously. The samples 1-50%-AC, 1-75%-AC, and 1-130%-AC were generated by dry grinding of 536.2 mg (2.882 mmol), 804.3 mg (4.323 mmol), and 1394.1 mg (7.493 mmol) of Cp₂Fe, respectively, with 1 g of DARCO.

NMR Instrumentation and Measurements. The ¹³C{¹H}, ²⁹Si{¹H} MAS, and static NMR experiments and also the static ²H NMR experiments were carried out with a Bruker Avance 400 solid-state NMR spectrometer (400 MHz for ¹H nuclei) equipped with a two-channel 7 mm MAS probe head. The standard single-pulse sequences (direct nuclear excitation with a 50° radio frequency pulse) were applied for the nuclei ¹³C and ²⁹Si using recycle delays as needed for the corresponding full spin–lattice relaxation estimated on the basis of inversion–recovery experiments.

The $^{13}\text{C}\{^1\text{H}\}$ MAS NMR experiment for 1, performed at a spinning rate of 3 kHz, required a recycle delay of 50 s due to the long ^{13}C relaxation time. The tppm15 (two-pulse phase modulation) pulse sequence has been used for complete ^1H decoupling. TMS (Me₄Si) has been used as an external standard for the ^{13}C and ^{29}Si chemical shifts and D₂O ($\delta(^2\text{H})$ 4.75 ppm) for referencing the ^2H NMR spectra.

The static ²H NMR data were collected with a solid-echo pulse sequence $(90^{\circ}-\tau-90^{\circ})^{19}$ with a τ delay of 40 μ s, a 90° pulse length of 5.25 μ s, and a relaxation delay of 4 s.

Typically 2000–2400 transients were recorded for all ²H solid-state NMR measurements. All samples were densely packed into the insetfree rotors as finely ground powders. Compressed nitrogen was used as both the bearing and drive gas for the MAS measurements.

The variable-temperature ^{13}C and ^2H NMR experiments have been performed with a standard temperature unit of the spectrometer calibrated with liquid methanol placed into a 7 mm rotor. The experimental ^{13}C and ^2H T_1 relaxation times were measured by inversion—recovery $(180^\circ - \tau - 90^\circ)$ experiments, and rf pulses were calibrated and τ delays widely varied to determine rough T_1 estimates. Relaxation (recycle) delays were adjusted to provide full nuclear relaxation in each cycle.

The quadrupolar coupling constants were derived from the 2H MAS NMR spectra using the NMR simulation program Dmfit. The error margin in this fitting procedure is $\pm 0.5~\mathrm{kHz}$.

The experimental 13 C and 2 H inversion—recovery data for the displays of signal intensity versus τ time have been treated with a standard nonlinear fitting computer program based on the Levenberg—Marquardt algorithm. 68 The statistical errors of the 13 C and 2 H T_{1} time determinations were <15%. The line-shape analysis of the static 13 C(1 H) and 2 H VT NMR spectra was performed with the program DNMR in the software package of the Bruker spectrometer.

AUTHOR INFORMATION

Corresponding Authors

Vladimir I. Bakhmutov — Department of Chemistry, Texas A&M University, College Station, Texas 77845-3012, United States; Email: bakhmoutov@chem.tamu.edu

Janet Blümel – Department of Chemistry, Texas A&M University, College Station, Texas 77845-3012, United States;

orcid.org/0000-0002-6557-3518; Phone: (+1)-979-845-7749; Email: bluemel@tamu.edu; Fax: (+1)-979-845-5629

Authors

Patrick J. Hubbard — Department of Chemistry, Texas A&M University, College Station, Texas 77845-3012, United States Jordon W. Benzie — Department of Chemistry, Texas A&M University, College Station, Texas 77845-3012, United States

Complete contact information is available at: https://pubs.acs.org/10.1021/acs.organomet.9b00800

Author Contributions

The manuscript was written through contributions of all authors. All authors have given approval to the final version of the manuscript.

Notes

The authors declare no competing financial interest.

ACKNOWLEDGMENTS

This work was supported by the National Science Foundation (CHE-1300208 and CHE-1900100). We thank Dr. Kyle J. Cluff for designing the graphical abstract.

REFERENCES

- (1) Hornbaker, D. J.; Kahng, S. J.; Misra, S.; Smith, B. W.; Johnson, A. T.; Mele, E. J.; Luzzi, D. E.; Yazdani, A. Mapping the One-Dimensional Electronic States of Nanotube Peapod Structures. *Science* **2002**, 295, 828–831.
- (2) Kaiser, K.; Scriven, L. M.; Schulz, F.; Gawel, P.; Gross, L.; Anderson, H. L. An sp-hybridized molecular carbon allotrope, cyclo[18]carbon. *Science* **2019**, *365*, 1299–1301.
- (3) Lee, J.; Kim, H.; Kahng, S. J.; Kim, G.; Son, Y. W.; Ihm, J.; Kato, H.; Wang, Z. W.; Okazaki, T.; Shinohara, H.; Kuk, Y. Bandgap modulation of carbon nanotubes by encapsulated metallofullerenes. *Nature* **2002**, *415*, 1005–1008.
- (4) Gupta, V. K.; Saleh, T. A. Sorption of pollutants by porous carbon, carbon nanotubes and fullerene- An overview. *Environ. Sci. Pollut. Res.* **2013**, *20*, 2828–2843.
- (5) Zhao, J.; Ren, W.; Cheng, H.-M. Graphene sponge for efficient and repeatable adsorption and desorption of water contaminations. *J. Mater. Chem.* **2012**, 22, 20197–20202.
- (6) Liu, T.; Li, Y.; Du, Q.; Sun, J.; Jiao, Y.; Yang, G.; Wang, Z.; Xia, Y.; Zhang, W.; Wang, K.; Zhu, H.; Wu, D. Adsorption of methylene blue from aqueous solution by graphene. *Colloids Surf.*, B **2012**, *90*, 197–203.
- (7) Zhao, G.; Li, J.; Ren, X.; Chen, C.; Wang, X. Few-Layered Graphene Oxide Nanosheets As Superior Sorbents for Heavy Metal Ion Pollution Management. *Environ. Sci. Technol.* **2011**, *45*, 10454–10462.
- (8) Yang, S.-T.; Chen, S.; Chang, Y.; Cao, A.; Liu, Y.; Wang, H. Removal of methylene blue from aqueous solution by graphene oxide. *J. Colloid Interface Sci.* **2011**, 359, 24–29.
- (9) Ren, X.; Chen, C.; Nagatsu, M.; Wang, X. Carbon nanotubes as adsorbents in environmental pollution management: A review. *Chem. Eng. J.* **2011**, *170*, 395–410.
- (10) Yang, K.; Xing, B. Adsorption of Organic Compounds by Carbon Nanomaterials in Aqueous Phase: Polanyi Theory and Its Application. *Chem. Rev.* **2010**, *110*, 5989–6008.
- (11) Hubbard, P. J.; Bakhmutov, V. I.; Blümel, J. Small Organic Molecules Adsorbed in the Pores of Activated Carbon: Molecular Motions and Interactions with the Surface. Manuscript in preparation.
- (12) Reisch, M. S. Carbon's Next Moves. Chem. Eng. News **2014**, 92, 18–19.
- (13) Cazetta, A. L.; Pezoti, O.; Bedin, K. C.; Silva, T. L.; Junior, A. P.; Asefa, T.; Almeida, V. C. Magnetic Activated Carbon Derived

- from Biomass Waste by Concurrent Synthesis: Efficient Adsorbent for Toxic Dyes. ACS Sustainable Chem. Eng. 2016, 4, 1058–1068.
- (14) Gil, M. V.; Alvarez-Gutierrez, N.; Martinez, M.; Rubiera, F.; Pevida, C.; Moran, A. Carbon adsorbents for CO_2 capture from biohydrogen and biogas streams: Breakthrough adsorption study. *Chem. Eng. J.* 2015, 269, 148–158.
- (15) Dubinin, M. M.; Vartapetyan, R. S.; Voloshchuk, A. M.; Kaerger, J.; Pfeifer, H. NMR study of translational mobility of molecules adsorbed on active carbons. *Carbon* 1988, 26, 515–520.
- (16) Heinen, A. W.; Peters, J. A.; van Bekkum, H. Competitive adsorption of water and toluene on modified activated carbon supports. *Appl. Catal., A* **2000**, *194*–*195*, 193–202.
- (17) Omichi, H.; Ueda, T.; Eguchi, T. Molecular motion of alcohols adsorbed in ACF hydrophobic nanoslits as studied by solid-state NMR. *Adsorption* **2015**, *21*, 273–282.
- (18) Park, J.; Hung, I.; Gan, Z.; Rojas, O. J.; Lim, K. H.; Park, S. Activated carbon from biochar: Influence of its physicochemical properties on the sorption characteristics of phenanthrene. *Bioresour. Technol.* **2013**, *149*, 383–389.
- (19) Fyfe, C. A. Solid-State NMR for Chemists; C.F.C. Press: Guelph, Canada, 1983.
- (20) Duncan, T. M. A Compilation of Chemical Shift Anisotropies; Farragut Press: Chicago, IL, 1990.
- (21) Selected examples: (a) Blümel, J. Linkers and catalysts immobilized on oxide supports: New insights by solid-state NMR spectroscopy. Coord. Chem. Rev. 2008, 252, 2410-2423. (b) Guenther, J.; Reibenspies, J.; Blümel, J. Synthesis, Immobilization, MAS and HR-MAS NMR of a New Chelate Phosphine Linker System, and Catalysis by Rhodium Adducts Thereof. Adv. Synth. Catal. 2011, 353, 443-460. (c) Silbernagel, R.; Diaz, A.; Steffensmeier, E.; Clearfield, A.; Blümel, J. Wilkinson-type hydrogenation catalysts immobilized on zirconium phosphate nanoplatelets. J. Mol. Catal. A: Chem. 2014, 394, 217-223. (d) Merckle, C.; Blümel, J. Improved Rhodium Hydrogenation Catalysts Immobilized on Oxidic Supports. Adv. Synth. Catal. 2003, 345, 584-588. (e) Merckle, C.; Blümel, J. Improved rhodium hydrogenation catalysts immobilized on silica. Top. Catal. 2005, 34, 5-15. (f) Baker, J. H.; Bhuvanesh, N.; Blümel, J. Tetraphosphines with tetra(biphenyl)silane and -stannane cores as rigid scaffold linkers for immobilized catalysts. J. Organomet. Chem. 2017, 847, 193-203. (g) Yang, Y.; Beele, B.; Blümel, J. Easily Immobilized Di- and Tetraphosphine Linkers: Rigid Scaffolds that Prevent Interactions of Metal Complexes with Oxide Supports. J. Am. Chem. Soc. 2008, 130, 3771-3773. (h) Pope, J. C.; Posset, T.; Bhuvanesh, N.; Blümel, J. The Palladium Component of an Immobilized Sonogashira Catalyst System: New Insights by Multinuclear HRMAS NMR Spectroscopy. Organometallics 2014, 33, 6750-6753. (i) Posset, T.; Blümel, J. New Mechanistic Insights Regarding Pd/Cu Catalysts for the Sonogashira Reaction: HRMAS NMR Studies of Silica-Immobilized Systems. J. Am. Chem. Soc. 2006, 128, 8394-8395. (j) Posset, T.; Guenther, J.; Pope, J.; Oeser, T.; Blümel, J. Immobilized Sonogashira catalyst systems: new insights by multinuclear HRMAS NMR studies. Chem. Commun. 2011, 47, 2059-2061. (k) Reinhard, S.; Soba, P.; Rominger, F.; Blümel, J. New Silica-Immobilized Nickel Catalysts for Cyclotrimerizations of Acetylenes. Adv. Synth. Catal. 2003, 345, 589-602. (1) Piestert, F.; Fetouaki, R.; Bogza, M.; Oeser, T.; Blümel, J. Easy one-pot synthesis of new dppm-type linkers for immobilizations. Chem. Commun. 2005, 1481-1483. (m) Cluff, K. J.; Bhuvanesh, N.; Blümel, J. Monometallic Ni(0) and Heterobimetallic Ni(0)/Au(I) Complexes of Tripodal Phosphine Ligands: Characterization in Solution and in the Solid State and Catalysis. Chem. - Eur. J. 2015, 21, 10138-10148. (n) Guenther, J.; Reibenspies, J.; Blümel, J. Synthesis and characterization of tridentate phosphine ligands incorporating long methylene chains and ethoxysilane groups for immobilizing molecular rhodium catalysts. Mol. Catal. 2019, 479, 110629.
- (22) (a) Iler, R. K. *The Chemistry of Silica*; Wiley: New York, 1979. (b) Blümel, J. Reactions of Ethoxysilanes with Silica: A Solid-State NMR Study. *J. Am. Chem. Soc.* 1995, 117, 2112–2113. (c) Behringer,

- K. D.; Blümel, J. Reactions of Ethoxysilanes with Silica: A Solid-State NMR Study. J. Liq. Chromatogr. Relat. Technol. 1996, 19, 2753–2765.
- (23) Oprunenko, Y.; Gloriozov, I.; Lyssenko, K.; Malyugina, S.; Mityuk, D.; Mstislavsky, V.; Günther, H.; Von Firks, G.; Ebener, M. Chromium tricarbonyl complexes with biphenylene as η^6 ligand: synthesis, structure, dynamic behaviour in solid state and thermal η^6, η^6 -haptotropic rearrangements. Experimental (NMR) and theoretical (DFT) studies. *J. Organomet. Chem.* **2002**, *656*, 27–42.
- (24) Hilliard, C. R.; Kharel, S.; Cluff, K. J.; Bhuvanesh, N.; Gladysz, J. A.; Blümel, J. Structures and Unexpected Dynamic Properties of Phosphine Oxides Adsorbed on Silica Surfaces. *Chem. Eur. J.* **2014**, 20, 17292–17295.
- (25) Kharel, S.; Cluff, K. J.; Bhuvanesh, N.; Gladysz, J. A.; Blümel, J. Structures and Dynamics of Secondary and Tertiary Alkylphosphine Oxides Adsorbed on Silica. *Chem. Asian J.* **2019**, *14*, 2704–2711.
- (26) Hilliard, C. R.; Bhuvanesh, N.; Gladysz, J. A.; Blümel, J. Synthesis, purification, and characterization of phosphine oxides and their hydrogen peroxide adducts. *Dalton Trans.* **2012**, *41*, 1742–1754.
- (27) Kharel, S.; Bhuvanesh, N.; Gladysz, J. A.; Blümel, J. New hydrogen bonding motifs of phosphine oxides with a silanediol, a phenol, and chloroform. *Inorg. Chim. Acta* **2019**, 490, 215–219.
- (28) Bewick, N. A.; Arendt, A.; Li, Y.; Szafert, S.; Lis, T.; Wheeler, K. A.; Young, J.; Dembinski, R. Synthesis and Solid-State Structure of (4-Hydroxy-3,5-diiodophenyl)phosphine Oxides. Dimeric Motifs with the Assistance of O-H···O = P Hydrogen Bonds. *Curr. Org. Chem.* **2015**, *19*, 469–474.
- (29) (a) Arp, F. F.; Ahn, S. H.; Bhuvanesh, N.; Blümel, J. Selective synthesis and stabilization of peroxides via phosphine oxides. *New J. Chem.* **2019**, 43, 17174–17181. (b) Arp, F. F.; Bhuvanesh, N.; Blümel, J. Hydrogen peroxide adducts of triarylphosphine oxides. *Dalton Trans.* **2019**, 48, 14312–14325.
- (30) (a) Ahn, S. H.; Lindhardt, D.; Bhuvanesh, N.; Blümel, J. Di(hydroperoxy)cycloalkanes Stabilized via Hydrogen Bonding by Phosphine Oxides: Safe and Efficient Baeyer—Villiger Oxidants. ACS Sustainable Chem. Eng. 2018, 6, 6829—6840. (b) Ahn, S. H.; Bhuvanesh, N.; Blümel, J. Di(hydroperoxy)alkane Adducts of Phosphine Oxides: Safe, Solid, Stoichiometric, and Soluble Oxidizing Agents. Chem. Eur. J. 2017, 23, 16998—17009. (c) Ahn, S. H.; Cluff, K. J.; Bhuvanesh, N.; Blümel, J. Hydrogen Peroxide and Di(hydroperoxy)propane Adducts of Phosphine Oxides as Stoichiometric and Soluble Oxidizing Agents. Angew. Chem., Int. Ed. 2015, 54, 13341—13345.
- (31) Cluff, K. J.; Schnellbach, M.; Hilliard, C. R.; Blümel, J. The adsorption of chromocene and ferrocene on silica: A solid-state NMR study. *J. Organomet. Chem.* **2013**, 744, 119–124.
- (32) Cluff, K. J.; Blümel, J. Adsorption of ferrocene on carbon nanotubes, graphene, and activated carbon. *Organometallics* **2016**, *35*, 3939–3948.
- (33) (a) Cluff, K. J.; Blümel, J. Adsorption of Metallocenes on Silica. *Chem. Eur. J.* **2016**, 22, 16562–16575. (b) Cluff, K. J.; Bhuvanesh, N.; Blümel, J. Adsorption of Ruthenium and Iron Metallocenes on Silica: A Solid-State NMR Study. *Organometallics* **2014**, 33, 2671–2680
- (34) Li, K.-T.; Yang, C.-N. Uniform rod-like self-assembly of polymer nanofibrils produced via propylene polymerization on Stober silica nuclei supported metallocene catalysts. *Mater. Today Commun.* **2019**, *19*, 80–86.
- (35) (a) Silveira, F.; Brambilla, R.; da Silveira, N. P.; do Carmo Martins Alves, M.; Stedile, F. C.; Pergher, S. B. C.; dos Santos, J. H. Z. Effect of textural characteristics of supported metallocenes on ethylene polymerization. *J. Mater. Sci.* **2010**, *45*, 1760–1768. (b) Silveira, F.; Alves, M. d. C. M.; Stedile, F. C.; Pergher, S. B.; dos Santos, J. H. Z. Microporous and mesoporous supports and their effect on the performance of supported metallocene catalysts. *J. Mol. Catal. A: Chem.* **2010**, *315*, 213–220.
- (36) Estrada-Ramirez, A. N.; Ventura-Hunter, C.; Vitz, J.; Díaz-Barriga Castro, E.; Peralta-Rodriguez, R. D.; Schubert, U. S.; Guerrero-Sánchez, C.; Pérez-Camacho, O. Poly(n-alkyl

- methacrylate)s as Metallocene Catalyst Supports in Nonpolar Media. *Macromol. Chem. Phys.* **2019**, 220 (19), 1900259.
- (37) Bernardes, A. A.; Scheffler, G. L.; Radtke, C.; Pozebon, D.; dos Santos, J. H. Z.; da Rocha, Z. N. Supported metallocenes produced by a non-hydrolytic sol-gel process: Application in ethylene polymerization. *Colloids Surf., A* **2020**, 584, 124020.
- (38) McKenna, W. P.; Bandyopadhyay, S.; Eyring, E. M. FT-IR/PAS Investigation of Chromocene Supported on Silica. *Appl. Spectrosc.* **1984**, *38*, 834–837 and references cited therein..
- (39) Karol, F. J.; Karapinka, G. L.; Wu, C.; Dow, A. W.; Johnson, R. N.; Carrick, W. L. J. Polym. Sci., Part A-1: Polym. Chem. 1972, 10, 2621.
- (40) Schnellbach, M.; Blümel, J.; Köhler, F. H. The Union Carbide catalyst (Cp₂Cr + SiO₂), studied by solid-state NMR. *J. Organomet. Chem.* **1996**, 520, 227–230.
- (41) Qiao, L.; Zhou, X.; Li, X.; Du, W.; Yu, A.; Zhang, S.; Wu, Y. Synthesis and performance of chiral ferrocene modified silica gel for mixed-mode chromatography. *Talanta* **2017**, *163*, 94–101.
- (42) Lowery, M. D.; Wittebort, R. J.; Sorai, M.; Hendrickson, D. N. Dynamics of ferrocene in a thiourea inclusion matrix. *J. Am. Chem. Soc.* 1990, 112, 4214–4225.
- (43) Narankiewicz, Z.; Blumenfeld, A. L.; Bondareva, V. L.; Mamedyarova, I. A.; Nefedova, M. N. Sokolov, Molecular motions and the structure of β -cyclodextrin inclusion complexes with ferrocene, (3)-Ferrocenophane-l,3-dione and ruthenocene. *J. Inclusion Phenom. Mol. Recognit. Chem.* **1991**, *11*, 233–245.
- (44) Pope, J.; Sue, H.-J.; Bremner, T.; Blümel, J. High-temperature steam-treatment of PBI, PEEK, and PEKK polymers with H_2O and D_2O : A solid-state NMR study. *Polymer* **2014**, *S5*, 4577–4585.
- (45) Pope, J. C.; Sue, H.-J.; Bremner, T.; Blümel, J. Multinuclear solid-state NMR investigation of the moisture distribution in PEEK/PBI and PEKK/PBI blends. *J. Appl. Polym. Sci.* **2015**, *132*, 1804–1816.
- (46) Günzler, H.; Gremlich, H.-U. IR-Spektroskopie, 4th ed.; Wiley-VCH: 2003.
- (47) Winter, W. K.; Curnutte, B., Jr.; Whitcomb, S. E. The infrared spectrum and structure of crystalline ferrocene. *Spectrochim. Acta* **1959**, *15*, 1085–1102.
- (48) Lippincott, E. R.; Nelson, R. D. The vibrational spectra and structure of ferrocene and ruthenocene. *Spectrochim. Acta* **1958**, *10*, 307–329.
- (49) Mohammadi, N.; Ganesan, A.; Chantler, C. T.; Wang, F. Differentiation of ferrocene D_{5d} and D_{5h} conformers using IR spectroscopy. *J. Organomet. Chem.* **2012**, *713*, 51–59.
- (50) Hoseinzadeh Hesas, R.; Arami-Niya, A.; Wan Daud, W. M. A.; Sahu, J. N. Preparation and characterization of activated carbon from apple waste by microwave-assisted phosphoric acid activation: Application in methylene blue adsorption. *BioResources* **2013**, *8*, 2950–2966.
- (51) Belgacem, A.; Belmedani, M.; Rebiai, R.; Hadoun, H. Characterization, Analysis and Comparison of Activated Carbons Issued from the Cryogenic and Ambient Grinding of Used Tires. *Chem. Eng. Trans.* **2013**, 32, 1705–1710.
- (52) Campbell, A. J.; Fyfe, C. A.; Harold-Smith, D.; Jeffrey, K. R. An Investigation of the dynamic structures of ferrocene, ruthenocene and dibenzenechromium in the solid state and in solution. *Mol. Cryst. Liq. Cryst.* **1976**, *36*, 1–23.
- (53) Kuwahara, D.; Imashiro, F.; Terao, T. Dynamics of ferrocene molecules enclathrated in P-cyclodextrin as studied by variable temperature one-dimensional SASS (switching-angle sample spinning) NMR spectroscopy. *Chem. Phys. Lett.* **1993**, 204, 533–537.
- (54) Holm, C. H.; Ibers, J. A. NMR Study of ferrocene, ruthenocene, and titanocene dichloride. *J. Chem. Phys.* **1959**, *30*, 885–888.
- (55) Orendt, A. M.; Facelli, J. C.; Jiang, Y. J.; Grant, D. M. NMR at cryogenic temperatures: a ¹³C NMR study of ferrocene. *J. Phys. Chem.* A **1998**, *102*, 7692–7697.
- (56) Massiot, D.; Fayon, F.; Capron, M.; King, I.; Le, C. S.; Alonso, B.; Durand, J.-O.; Bujoli, B.; Gan, Z.; Hoatson, G. Modelling one- and

- two-dimensional solid-state NMR spectra. Magn. Reson. Chem. 2002, 40, 70-76.
- (57) Ormaza, M.; Abufager, P.; Bachellier, N.; Robles, R.; Verot, M.; Le Bahers, T.; Bocquet, M.-L.; Lorente, N.; Limot, L. Assembly of ferrocene molecules on metal surfaces revisited. *J. Phys. Chem. Lett.* **2015**, *6*, 395–400.
- (58) Kempiński, M.; Śliwińska-Bartkowiak, M.; Kempiński, W. Molecules in the porous system of activated carbon fibers spin population control. *Rev. Adv. Mater. Sci.* **2007**, *14*, 163—166.
- (59) Wieckowski, A. B.; Najder-Kozdrowska, L.; Rechnia, P.; Malaika, A.; Krzyzynska, B.; Kozłowski, M. EPR Characteristics of activated carbon for hydrogen production by the thermo-catalytic decomposition of methane. *Acta Phys. Pol., A* **2016**, *130*, 701–704.
- (60) Xu, Y.; Watermann, T.; Limbach, H.-H.; Gutmann, T.; Sebastianib, D.; Buntkowsky, G. Water and small organic molecules as probes for geometric confinement in well-ordered mesoporous carbon materials. *Phys. Chem. Chem. Phys.* **2014**, *16*, 9327–9336.
- (61) Harris, P. J. F.; Liu, Z.; Suenaga, K. Imaging the atomic structure of activated carbon. *J. Phys.: Condens. Matter* **2008**, 20, 362201–362206.
- (62) Chiang, H. L.; Huang, C. P.; Chiang, P. C. The Adsorption of Benzene and Methylethylketone onto Activated Carbon: Thermodynamic aspects. *Chemosphere* **2002**, *46*, 143–152.
- (63) Parida, S. K.; Dash, S.; Patel, S.; Mishra, B. K. Adsorption of organic molecules on silica surface. *Adv. Colloid Interface Sci.* **2006**, 121, 77–110.
- (64) Hernandez, M. A.; Velasco, J. A.; Asomoza, M.; Solís, S.; Rojas, F.; Lara, V. H. Adsorption of benzene, toluene, and *p*-xylene on microporous SiO₂. *Ind. Eng. Chem. Res.* **2004**, *43*, 1779–1787.
- (65) Zhao, Z. G.; Zhang, L. H.; Lin, Y. Thermodynamics of adsorption of organic compounds at the silica gel/nonpolar solvent interfaces. *J. Colloid Interface Sci.* **1994**, *166*, 23–28.
- (66) Russo, P. A.; Ribeiro Carrott, M. M. L.; Carrott, P. J. M. Adsorption of toluene, methylcyclohexane and neopentane on silica MCM-41. *Adsorption* **2008**, *14*, 367–375.
- (67) Bishop, J. J.; Davison, A.; Katcher, M. L.; Lichtenberg, D. W.; Merrill, R. E.; Smart, J. C. Symmetrically disubstituted ferrocenes: I. The synthesis of potential bidentate ligands. *J. Organomet. Chem.* **1971**, *27*, 241–249.
- (68) Levenberg, K. A Method for the Solution of Certain Non-Linear Problems in Least Squares. Q. Appl. Math. 1944, 2, 164–168.